

Natural Flavonoid Glycoside-Based Zinc Oxide Nanoparticles: Compound Isolation, Nanoparticle Green Synthesis, Characterization, and *in vitro* Antioxidant, Anti-hyperglycaemic and Anti-inflammatory Effects

Pallab Kar^{1,*}, Ayodeji O. Oriola^{2,*}, Adebola O. Oyedeji^{1,2}

Pallab Kar^{1,*}, Ayodeji O. Oriola^{2,*},
Adebola O. Oyedeji^{1,2}

¹African Medicinal Flora and Fauna Research Niche Area, Walter Sisulu University Nelson Mandela Drive, P/Bag X1, Mthatha 5117, SOUTH AFRICA.

²Department of Chemical and Physical Sciences, Walter Sisulu University, Nelson Mandela Drive, P/Bag X1, Mthatha 5117, SOUTH AFRICA.

Correspondence

P. Kar

African Medicinal Flora and Fauna Research Niche Area, Walter Sisulu University Nelson Mandela Drive, P/Bag X1, Mthatha 5117, SOUTH AFRICA.

E-mail: pallabkar.bio@gmail.com

A.O. Oriola

Department of Chemical and Physical Sciences, Walter Sisulu University, Nelson Mandela Drive, P/Bag X1, Mthatha 5117, SOUTH AFRICA.

E-mail: aooriola@gmail.com

History

- Submission Date: 28-08-2025;
- Review completed: 03-09-2025;
- Accepted Date: 21-10-2025.

DOI : 10.5530/pj.2025.17.66

Article Available online

<http://www.phcogj.com/v17/i5>

Copyright

© 2025 Phcogj.Com. This is an open-access article distributed under the terms of the Creative Commons Attribution 4.0 International license.

ABSTRACT

Introduction: Recent advances in effective and efficient drug delivery have favoured the biological applications of phytochemical-based metal oxide nanoparticles (NPs). **Objective:** This study, therefore, utilized a flavonoid glycoside, Myricitrin (MY), isolated from *Eugenia uniflora* as a biogenic substance for the synthesis of zinc oxide nanoparticles (ZnONPs) and evaluated the antioxidant, anti-hyperglycaemic, and anti-inflammatory potentials. **Materials and Methods:** Flavonoid glycoside was isolated from the leaf of *E. uniflora* following standard phytochemical techniques for extraction, solvent-partitioning, column chromatography, and thin-layer chromatography. The phytocompound was characterized by NMR and HRESI-MS methods. Zinc oxide NPs were green synthesized using the isolated flavonoid glycoside. The biogenic ZnONPs were characterized using UV-Vis, FESEM, EDX, and XRD techniques. The biological potential of the MY-ZnONPs was based on *in vitro* analysis. Nitric oxide (NO), H₂O₂, OH, and O₂⁻ antioxidant methods were used. The anti-hyperglycaemic effect was based on α -amylase and α -glucosidase enzyme inhibition, while the egg albumin denaturation (EAD) method was used to determine the anti-inflammatory effect. **Results:** Flavonoid glycoside was isolated and characterized as myricitrin from *E. uniflora*. The MY-ZnONPs were green synthesized as a greyish powder. The UV-Vis absorption peaks at 387 and 415 nm match the characteristic peaks for ZnONPs. The FESEM revealed petal-, irregular-, and spindle-shaped NPs of 30-80 nm size, which tend to agglomerate in clusters and bundles. The EDX analysis showed the elemental weight percentage of Zn and O to be 79.83% and 18.51%, respectively, indicating the successful formation of ZnO nanoparticles. The X-ray diffractogram showed the crystallinity of the NPs at 29.23^o, 36.25^o, 51.50^o, 63.67^o, 72.06^o, and 78.90^o. At 100 μ g/mL, the NPs demonstrated a comparable 68% inhibition of O₂⁻ to Quercetin, the standard antioxidant. They inhibited EAD in a dose-dependent manner, having \geq 75% inhibition at 200 μ g/mL. Finally, they exhibited notable anti-hyperglycaemic properties against α -amylase and α -glucosidase with IC₅₀ of 89.24 \pm 0.63 and 105.95 \pm 0.05 μ g/mL, respectively. **Conclusion:** This study has shown MY-ZnONPs as a flavonoid glycoside-based metal oxide nanoparticle with notable antioxidant, anti-diabetic, and anti-inflammatory activities.

Keywords: Green synthesis, natural flavonoid glycosides, ZnO nanoparticles, antioxidant, anti-hyperglycaemia, anti-inflammation.

INTRODUCTION

The innovative process of plant-mediated synthesis of nanoparticles (NPs) has numerous uses in the food industry, medicine, and agriculture. The toxicity of NPs produced using traditional procedures limits their clinical applications. Because of the physico-chemical characteristics of plant-based NPs, this approach extends the NPs' lifespan, which gets around the drawbacks of traditional chemical and physical NP synthesis methods¹⁻³. Many biomolecules and metabolites, including proteins, vitamins, and intermediates based on coenzymes, phenols, flavonoids, and carbohydrates, are genetically diverse in plants. These plant metabolites have functional groups such as amine (NH), carbonyl (C=O), and hydroxyl (OH) that react with metal ions to shrink them into nanoscale particles. In particular, flavonoids have interesting functional groups, with the OH group of flavonoids thought to be primarily in

charge of reducing metal ions into NPs⁴. Besides aiding in the bio-reduction of ions to nanoscale size, these molecules are essential for the capping of nanoparticles, which is necessary for stability and biocompatibility⁵. In a single process, reducing agents such as sterols, alkaloids, phenolics, and flavonoids can convert metal ions into NPs⁶. Using plant extracts from different plant species, some metals, including copper (Cu), gold (Au), and silver (Ag), have been widely employed for the biosynthesis of NPs⁷⁻⁹. Their more significant toxicity to people and animals, however, seriously restricts their application in the medical field. Rarely does the inorganic compound zinc oxide appear in nature. It usually exists in crystalline form. Manganese impurities cause naturally occurring zinc oxide's characteristic red or orange coloration¹⁰. After purification, ZnO is a greyish-to-whitish powder that is essentially water-insoluble. Because of their size-dependent characteristics and low toxicity, ZnONPs have been extensively used in various fields, including

Cite this article: Pallab K, Ayodeji O O, Adebola O O. Natural Flavonoid Glycoside-Based Zinc Oxide Nanoparticles: Compound Isolation, Nanoparticle Green Synthesis, Characterization, and *in vitro* Antioxidant, Anti-hyperglycaemic and Anti-inflammatory Effects. Pharmacogn J. 2025;17(5): 531-541.

microelectronics, textiles, diagnostics, cosmetics, and medicine¹¹. For the biosynthesis of NPs for therapeutic applications, ZnO has been discovered to be more effective and potentially helpful than other metals¹². Numerous investigations have shown how to synthesize ZnONPs utilizing various plant extracts. To create ZnONPs, for instance, a leaf extract from *Hibiscus rosasinensis* and floral extract from the medicinal plant *Cassia auriculata* were employed as reducing agents for zinc nitrate^{13,14}. One naturally occurring dietary flavonoid frequently found in fruit, vegetables, tea, and herbal treatments is myricitrin (MY). Biological activities are linked to MY, including antibacterial, antiviral, antioxidant, anti-inflammatory, anticancer, urease suppression, and many more¹⁵⁻¹⁹. Thus, MY is being explored as a candidate biological ingredient in the food, cosmetics, and pharmaceutical industries²⁰.

Eugenia uniflora L. (Myrtaceae) is a medicinal plant used in African and Asian folkloric medicines to remedy chronic inflammatory ailments such as diabetes and rheumatoid arthritis²¹. Studies have shown that the *E. uniflora* leaves contain flavonoids and glycosides, including MY²². Therefore, this study presents a new method for separating and characterizing MY from *Eugenia uniflora* and creating eco-friendly ZnONPs, which turn metal ions into nanoparticles without the use of dangerous chemicals. Energy-dispersive X-ray spectroscopy (EDX), field emission scanning electron microscopy (FESEM), and ultraviolet (UV) were used to characterize the produced nanoparticles. Additionally, the antioxidant, anti-hyperglycaemic, and anti-inflammatory properties of flavonoid glycoside-based ZnONPs were investigated.

MATERIALS AND METHODS

Plant material

In March 2021, while at Obafemi Awolowo University (O.A.U.), Ile-Ife, Nigeria (GPS coordinates: N 7° 31'03.799200, E 4° 31'03.852800), *Eugenia uniflora* leaves were gathered. The collection was verified at the Ife Herbarium, O.A.U., Ile-Ife, using voucher IFE 16589. The leaves in the screen house turned frequently as they air-dried away from the direct sunlight and detached from their branches. Powdered, the dried leaves were stored for later use in an airtight plastic bag.

Isolation of flavonoid glycoside from *E. uniflora* leaf

A flavonoid glycoside was isolated from the leaf powder of *E. uniflora* following the method of Oriola *et al.*²². The leaf powder (500 g) was extracted with 3 L of 80% ethanol mixed with 20% distilled water. The extraction was refluxed at 60 °C for 4 h. It was allowed to cool, then filtered and concentrated to dryness *in vacuo* on a rotary evaporator (Heidolph 110 Instruments GmbH & Co. KG, Schwabach, Germany). The afforded extract (62 g) was suspended in 200 mL of distilled water and partitioned with n-hexane (2 × 400 mL), dichloromethane (DCM, 3 × 400 mL), and ethyl acetate (EtOAc, 4 × 400 mL). The EtOAc fraction (10 g) was solubilized in acetone and adsorbed to 20 g silica gel. An open-column chromatography was set up for the elution process, with 100 g silica as the separating layer. The elution was performed in a gradient manner as thus: n-Hexane (Hex, 100%, 500 mL), Hex-EtOAc (9:1, 8:2, 6:4, 4:6, 2:8, 500 mL each), EtOAc-MeOH (95:5, 9:1, 8:2, 7:3, 5:5, 3:7, 500 mL each). The elution phase afforded forty-three column fractions, each collected in a 500 mL flask. Thin-layer chromatography (TLC) analysis was performed on the column fractions and with reference to standard Myricitrin (Sigma-Aldrich, St Louis, MO, USA) to monitor the compound isolation. Thereafter, the column fractions were bulked into six subfractions E1–E6. Subfraction E5 was further fractionated using an isocratic elution with DCM-MeOH (7:3) on a Sephadex LH-20 column, affording E5a–d. Subfraction E5b gave a yellow amorphous solid (27 mg), with a single yellow spot (R_f 0.49). The yellow spot became charred upon spraying with 10% sulfuric acid and heated at 105 °C, suggesting a flavonoid glycoside compound. The compound exhibited a melting point range of 196–197 °C.

Characterization of isolated flavonoid glycoside

The isolated flavonoid glycoside was analyzed on the Avance 600 MHz Nuclear Magnetic Resonance Spectrometer (Bruker Biospin GmbH-Rheinstetten, Germany) and the Quadrupole Time-of-Flight (QToF) Synapt G2 Mass Spectrometer (Waters Corporation, Milford, MA, USA) at the Central Analytical Facility, Stellenbosch University, South Africa. Full NMR data were acquired in DMSO- d_6 (Sigma-Aldrich Chemie GmbH, Taufkirchen, Germany) at 0-14 and 0-220 ppm on the ¹H and the ¹³C nuclei, respectively, with tetramethyl silane as an internal standard. Mass determination was performed using the electrospray ionization method (HRESI-MS). The molecular weight of MY was expressed in mass-to-charge ratio (m/z).

Green Synthesis of ZnONPs using a natural flavonoid glycoside (myricitrin)

The isolated flavonoid glycoside elucidated as myricitrin (MY) was used as a bio-reducing agent to prepare ZnONPs. Briefly, MY (15 mg dissolved in 5 mL of distilled water) was added to 100 mL of 0.2 M zinc acetate dihydrate solution (4.3898 g in 100 mL distilled water) and heated to 100 °C for 4 h under continuous stirring at 250 rpm. A slightly higher temperature was used to synthesize nanoparticles, as it is proven to produce small-sized, uniform nanoparticles²³. The colour shift in the solution indicates the formation of zinc oxide nanoparticles. After the incubation, the solution was centrifuged at 10,000 rpm for 10 min. The afforded MY-ZnONPs were washed with distilled water, centrifuged again, and dried in a hot oven at 60 °C. Completely dried nanoparticles were stored at 4 °C.

Characterization of biogenic zinc oxide nanoparticles

UV-Visible spectra analysis

Characterization of biogenically synthesized nanoparticles was done by UV-visible spectroscopy after 24 h of the experiment, and a graph was also plotted.

Field emission scanning electron microscope (FESEM)

The powdered samples were placed on copper mesh for FESEM investigation, and a gold sputtering apparatus was applied with a 3 nm gold coating. FESEM (German manufacturer Carl Zeiss; model: SIGMA-0261) was used to record the surface morphology of the ZnONPs at a 3 kV accelerating voltage at 20,000 × magnification.

Energy-dispersive X-ray spectroscopy (EDX)

To determine the presence of elemental Zn, energy dispersive X-ray spectroscopy (EDX) was done using a Scanning Electron Microscope (JEOL JSM-IT100InTouchScope™, Tokyo, Japan) equipped with Oxford-EDX software. The powdered dried nanoparticles were mounted on copper mesh, and a 3 nm gold coating was done by a gold sputtering unit. Eighty mm² SDD detectors that detect elements under high resolution were used for the purpose.

X-ray diffraction analysis (XRD)

An EMPYREAN machine (Make PAN analytical, Netherlands) with CuK α radiation ($\lambda=1.54584\text{\AA}$) and 40 kV voltage and 30mA current was used to investigate X-ray diffraction. The crystalline structure was ascertained by comparing the acquired data with the standard JCPDS library. The Debye-Scherrer equation, which reads $D = (0.9\lambda/\beta \cos\theta)$, has been used to determine the average size of the crystalline structure. In this equation, D represents the diameter of the crystallite size, λ the wavelength for CuK α , β the full width at half-maximum (FWHM), and θ the Bragg diffraction.

Determination of *in vitro* antioxidant activity of biogenic zinc oxide nanoparticles

Nitric oxide (NO) radical scavenging assay

The quantification technique of the Griess-Ilosvoy reaction at physiological pH was used to measure the nitric oxide radical scavenging activity with minor adjustments²⁴. Briefly, phosphate-buffered saline (pH 7.4), sodium nitroprusside (SNP; 10 mM), and different concentrations of MY-ZnONPs (0-200 µg/mL) were mixed and made the final volume of 3 mL. After the mixture was thoroughly vortexed and incubated for 150 min at 25 °C, 0.5 mL of the pre-incubated reaction mixture was mixed with 1 mL of sulfanilamide (0.33%), which was diluted in 20% glacial acetic acid and allowed to sit at room temperature for 5 min. To facilitate colour production, 1 mL of N-(1-Naphthyl) ethylenediamine dihydrochloride (NEED; 0.1%) was added, and the mixture was kept at 25 °C for 30 min. The absorbance was measured at 540 nm using distilled water as a blank. Curcumin functioned as a standard reference. The percent of inhibition was calculated according to the following equation I:

$$\text{The equation I: Percentage of scavenging} = \frac{A_0 - A_1}{A_0} \times 100$$

Where, A_0 = absorbance of the control and A_1 = absorbance in the presence of samples and standard.

Hydrogen peroxide scavenging assay

The hydrogen peroxide (H_2O_2) scavenging capacity was calculated using a modified version of Long *et al.*²⁵. H_2O_2 (50 mM) and different concentrations of MY-ZnONPs (0-200 µg/mL) were combined in a screw-capped bottle, and the mixture was allowed to dark-incubate for 30 min at room temperature (≈ 25 °C). Next, 90 µL of H_2O_2 , 10 µL of HPLC-grade methanol, and 0.9 ml of FOX reagent (made by combining 9 volumes of 4.4 mM BHT in HPLC-grade methanol with 1 volume of 1 mM xylenol orange and 2.56 mM ammonium ferrous sulfate in 0.25 M H_2SO_4) were added. After giving the mixture a gentle vortex and letting it sit for 30 min, the absorbance at 560 nm was determined. Ascorbic acid was utilized as a positive control. The percentage inhibition was calculated as before using equation I.

Hydroxyl radical scavenging assay

Hydroxyl radical scavenging activity was conducted using the Fenton reaction model with a small modification²⁶. 2-deoxy-2-ribose (2.8 mM), monopotassium phosphate-potassium hydroxide buffer (KH_2PO_4 -KOH; 20 mM; pH 7.4), $FeCl_3$ (100 µM), ethylene diamine tetraacetic acid (EDTA; 100 µM), hydrogen peroxide (H_2O_2 ; 1.0 mM), ascorbic acid (100 µM), and varying concentrations of MY-ZnONPs (0-200 µg/mL) were added to the reaction mixture until a final volume of 1 mL was achieved. After carefully mixing the reaction mixture, it was incubated for 60 min at 37 °C. Following the completion of the incubation period, the 0.5 ml mixture was carefully transferred into a fresh tube and mixed with 1 mL each of aqueous thiobarbituric acid (TBA; 1%) and TCA (2.8%). Once more, the finished mixture was incubated for 15 min at 90 °C. The absorbance at 532 nm was measured after the mixture had cooled to room temperature in comparison to an appropriate blank solution. A positive control was employed as ascorbic acid. The percentage inhibition was calculated as before using equation I.

Superoxide radical scavenging assay

The assay was conducted in accordance with Fontana *et al.*²⁷. The nitro-blue tetrazolium (NBT) is reduced to purple formazan in the presence of the nonenzymatic PMS/NADH system, which produces superoxide radicals when exposed to oxygen. Phosphate buffer (20 mM, pH 7.4), NBT (50 µM), PMS (15 µM), NADH (73 µM), and varying doses (0-200 µg/mL) MY-ZnONPs were combined to create a reaction mixture

(1 ml). After gently vortexing the mixtures, they were incubated for five min at room temperature. The amount of formazan produced was estimated by measuring the absorbance at 562 nm compared to the equivalent blank samples. Quercetin served as a positive control. The percentage inhibition was calculated as before using equation I.

In vitro anti-hyperglycaemic activities of the MY-ZnONPs

α -Amylase inhibition

The α -amylase inhibitory activities of the MY-ZnONPs were carried out following a modified procedure published by Wickramaratne *et al.*²⁸. In brief, the MY-ZnONPs were dissolved in 5% DMSO and were further thawed in phosphate buffer (0.02 M, pH 6.9) containing 0.006 M NaCl to yield varying concentrations. Then, an equal volume (250 µL) of α -amylase (from *Aspergillus oryzae*) enzyme solution (2 U/mL) and the MY-ZnONPs were mixed in a test tube, and the resultant mixture was incubated for 10 min at room temperature. Afterward, 1% starch solution (250 µL) in the same phosphate buffer was added to the mixture to initiate the reaction, and the resultant solution was further incubated for 10 min at 25 °C. Thereafter, the reaction was put to a halt by adding 1 mL 3,5-dinitrosalicylic acid (DNSA) reagent, and the mixture was subsequently boiled in a water bath for 10 min at 95 °C, cooled at room temperature, and 3 mL of distilled water was finally added just before measuring the OD at 540 nm. The standard acarbose and control were prepared following the steps above. The enzyme inhibition percentage was calculated with the equation shown below.

$$\% \text{ Inhibition of } \alpha - \text{ amylase} = \frac{ABS_{\text{control}} - ABS_{\text{sample}}}{ABS_{\text{control}}} \times 100$$

α -Glucosidase inhibition

The α -glucosidase inhibitory activities of the MY-ZnONPs were estimated, as explained by Rengasamy *et al.*²⁹. Briefly, in 96-well microplates, equal volumes (20 µL) of MY-ZnONPs dissolved in dimethyl sulfoxide (DMSO) at different concentrations and yeast α -glucosidase (0.1 U/mL) in phosphate buffer (0.1 M, pH 6.8) were mixed. Then, 40 µL of the substrate [0.375 mM p-nitrophenyl- α -D-glucopyranoside (pNPG) in 0.1 M phosphate buffer at pH 6.8] was added to the mixture to initiate the reaction. Thereafter, the reaction mixture was incubated for 40 min at 37 °C. Subsequently, after the incubation period, 80 µL of 0.2 M sodium carbonate in potassium phosphate buffer (0.1 M, pH 6.8) was added to each well to halt the reaction. The intensity of the colour change in the reaction mixture signifies the amount of p-nitrophenyl produced, and the OD was measured at 405 nm. Wells containing phosphate buffer instead of sample extracts were considered the control, whereas acarbose was used as a standard. The enzyme inhibition percentage was calculated as follows:

$$\% \text{ Inhibition of } \alpha - \text{ glucosidase} = \frac{ABS_{\text{control}} - ABS_{\text{sample}}}{ABS_{\text{control}}} \times 100$$

In vitro anti-inflammatory study on MY-ZnONPs

The *in vitro* anti-inflammatory properties of MY-ZnONPs were determined by their inhibitory effect on protein denaturation using the egg albumin denaturation assay with slight modification³⁰. A 0.2 ml of albumin from a fresh chicken egg, 2.8 mL of phosphate buffer saline at pH 6.4, and 2 mL of MY-ZnONPs at 12.5, 25, 50, 100, and 200 µg/mL concentrations were mixed in three replicates. The reaction mixture was incubated at 37 °C for 15 min away from direct light. Then, it was boiled at 70 °C for 5 min in a thermostatic water bath. The resulting mixture was allowed to cool before the absorbance was

measured at 655 nm wavelength. Diclofenac was used as the reference anti-inflammatory drug. The percentage inhibitory effect of essential oils on egg albumin denaturation (EAD) was calculated according to the following equation I:

$$\% \text{ Inhibition of EAD} = \frac{ABS_{\text{control}} - ABS_{\text{sample}}}{ABS_{\text{control}}} \times 100$$

Where, EAD = egg albumin denaturation, ABS = absorbance

Statistical analysis

To compare the activity of MY-ZnONPs and references, Student's t-Test integrated with the KyPlot program (version 5.0) was used for statistical analysis.

RESULTS AND DISCUSSION

Spectra data on isolated flavonoid glycoside

HR-ESI-MS (*m/z*, % rel. int.): *m/z* 465.1033 ($C_{21}H_{20}O_{12}$), found *m/z* 465.1022 $[M+H]^+$ (100%); *m/z* 319.0454 ($C_{15}H_{11}O_8$), found 319.0441 $[M-Rhamnosyl]^+$ (89%); **¹H NMR** (600 MHz, DMSO-*d*₆) δ 0.85 (3H, *d*, *J* = 6.1 Hz, H-6"), 3.15 (1H, *t*, *J* = 9.3 Hz, H-4"), 3.36 (1H, *dq*, *J* = 5.1, 6.5 Hz, H-5"), 3.56 (1H, *dd*, *J* = 2.5, 4.5 Hz, H-3"), 3.98 (1H, *d*, *J* = 3.3 Hz, H-2"), 5.20 (1H, *s*, H-1"), 6.20 (1H, *d*, *J* = 2.5 Hz, H-6), 6.37 (1H, *d*, *J* = 2.5 Hz, H-8), 6.91 (2H, *d*, *J* = 6.9 Hz, H-2', H-6'); **¹³C NMR** (150 MHz, DMSO-*d*₆): δ 157.5 (C-2), 134.3 (C-3), 177.8 (C-4), 104.1 (C-4a), 161.4 (C-5), 98.7 (C-6), 164.2 (C-7), 93.6 (C-8), 156.5 (C-8a), 119.6 (C-1'), 107.9 (C-2'/6'), 145.8 (C-3'/5'), 136.5 (C-4'), *L*-Rhamnose: 101.9 (C-1"), 70.0 (C-2"), 70.4 (C-3"), 71.3 (C-4"), 70.6 (C-5"), 17.5 (C-6").

Structure elucidation of isolated flavonoid glycoside

The presence of three aromatic protons δ_H 6.20, 6.37, and two chemically equivalent protons at δ_H 6.91, and the most deshielded signals at δ_H 12.68 in the ¹H NMR spectrum suggests a flavonoid compound (Figure 1A). Six signals at δ_H 5.21–0.85 further revealed the presence of one pyranose sugar attachment to make a flavonoid glycoside. The ¹³C NMR showed twenty-one signals, suggesting a C₂₁ flavonoid compound (Figures 1B and C). The most deshielded signal resonated at δ_C 177.8, indicating the presence of a carbonyl functional group of a ketone, which is typical of an enone at position C-4 of a flavonoid. The HSQC spectrum showed the rhamnose carbon signals with the anomeric carbon (C-1") resonating at δ_C 101.9, and the C-2 to C-5 signals at δ_C 70.0–71.3. In the HMBC spectrum, a three-bond correlation (³J_{CH}) was observed between the methyl proton at H-6" (δ_H 0.85) and the C-4" signal (δ_C 71.3), confirming the presence of a rhamnose sugar unit. Additionally, the 3-O-rhamnosyl linkage was confirmed in the HMBC experiment, with a long-range coupling between the anomeric proton (H-1") at δ_H 5.17 and the C-3 of the flavonoid core at δ_C 134.3. The acquired NMR spectral data agreed with that of Myricetin-3-O- α -L-rhamnopyranoside, a flavone glycoside reported by Kassem *et al.*³⁰ and Oriola *et al.*²². The HR-ESI-MS data agreed with the NMR elucidated Myricetin-3-O-rhamnoside structure. The mass fragmentation pattern showed a quasi-molecular ion $[M+H]^+$ peak at *m/z* 465.1022, consistent with the molecular formula C₂₁H₂₀O₁₂ for Myricitrin. The daughter ion at *m/z* 319.0441 indicates a homolytic cleavage of rhamnosyl ion $[M-146]^+$, affording the Myricetin flavonoid core (Figure 2).

Characterization of biogenic zinc oxide nanoparticles

UV-Visible spectra analysis

The green synthesized MY-ZnONPs' UV-Vis spectrum is shown in Figure 3. The starting material (zinc precursor) for zinc acetate dihydrate displayed absorption peaks at 208–238 nm, characteristic of

zinc acetate's UV-vis absorption peaks^{31,32}. Additionally, the absorption peaks in the MY-ZnONPs at 387 and 415 nm match the characteristic peaks for ZnONPs, suggesting that ZnONPs were successfully formed^{33–35}.

Field emission scanning electron microscope (FESEM)

FESEM results revealed that green synthesis of MY-ZnONPs led to the formation of uniquely shaped flavonoid glycoside-mediated ZnONPs, notably as petal-, irregular-, and spindle-shaped NPs, which tend to agglomerate in clusters and bundles (Figure 4). The average size of NPs ranges between 30–80 nm³⁶.

Energy-dispersive X-ray spectroscopy (EDX)

The elemental makeup of the MY-ZnONPs was ascertained in this study using EDX analysis. The spectrum demonstrated the presence of O, Al, Si, Fe, and Zn (Figure 5). The weight percentage values of 79.83 and 18.51% for the Zn and O components of the NPs, respectively, are consistent with earlier findings on green-produced ZnO NPs^{37,38}. Additionally, the surface plasmon resonance effect, which is common for the absorption of ZnO nanostructures, is responsible for the distinctive Zn peaks in the obtained EDX spectrum at 1.11, 8.55, and 9.23 keV³⁹.

X-ray diffraction analysis (XRD)

The crystallinity of the biosynthesized ZnONPs can be inferred from the X-ray diffraction pattern obtained and shown in Figure 6. Peaks at 29.23°, 36.25°, 51.50°, 63.67°, 72.06°, and 78.90° were found in the sample's X-ray diffraction (XRD) investigation; these have been indexed as (99), (100), (101), (108), (102), and (103) accordingly. The diffraction pattern's observed intensity peaks follow the standard JCPD No00-036-1451 and the hexagonal wurtzite structure described for ZnONPs. Furthermore, these diffraction peaks indicate that the biosynthesized ZnONPs are crystalline rather than amorphous.

Determination of *in vitro* antioxidant activity

Nitric oxide is an essential signaling molecule; too much can damage cells and tissues by acting as reactive oxygen species (ROS). MY-ZnONPs demonstrated dose-dependent nitric oxide scavenging activity (61.79 ± 1.22 percent at 200 µg/mL) compared to conventional curcumin. In living organisms, nitric oxide and zinc oxide nanoparticles work together to prevent excessive nitric oxide accumulation that might damage membranes (Figure 7A). Hydrogen peroxide (H₂O₂) is produced in peroxisomes by the combination of superoxide anion and superoxide dismutase (SOD). The hydroxyl radical (OH•) created when H₂O₂ accumulates in cells and combines with other transition metals like Fe²⁺, Cu²⁺, etc., can harm DNA and result in lipid peroxidation⁴⁰. Compared to ascorbic acid as a reference, MY-ZnONPs showed a notable H₂O₂ scavenging activity (79.07 ± 0.56 % at 200 µg/mL) (Figure 7B)⁴¹. Proteins and DNA are examples of biological macromolecules that are harmed by superoxide anions (O₂•⁻). When oxidative stress is high, the superoxide anion, a less reactive free radical, can create more reactive species *in vivo*. The produced MY-ZnONPs resulted in a concentration-dependent increase in superoxide radical scavenging activity (80.74 ± 0.93 % at 200 µg/mL) (Figure 7C). By neutralizing hydroxyl radicals, MY-ZnONPs (79.74 ± 1.04 % at 200 µg/mL) shield cells and help to establish a stable cellular environment (Figure 7D). Accordingly, recent studies indicate that MY-ZnONPs might be crucial for the recovery from oxidative stress-related diseases.

In vitro anti-hyperglycaemic activities of the MY-ZnONPs

Hyperglycaemia, or elevated blood sugar, is a consequence of diabetes mellitus (DM), a metabolic disease caused by insufficient insulin secretion or activity while metabolizing carbohydrates, fats, and proteins^{42–44}. Many antidiabetic medications are available. However, they

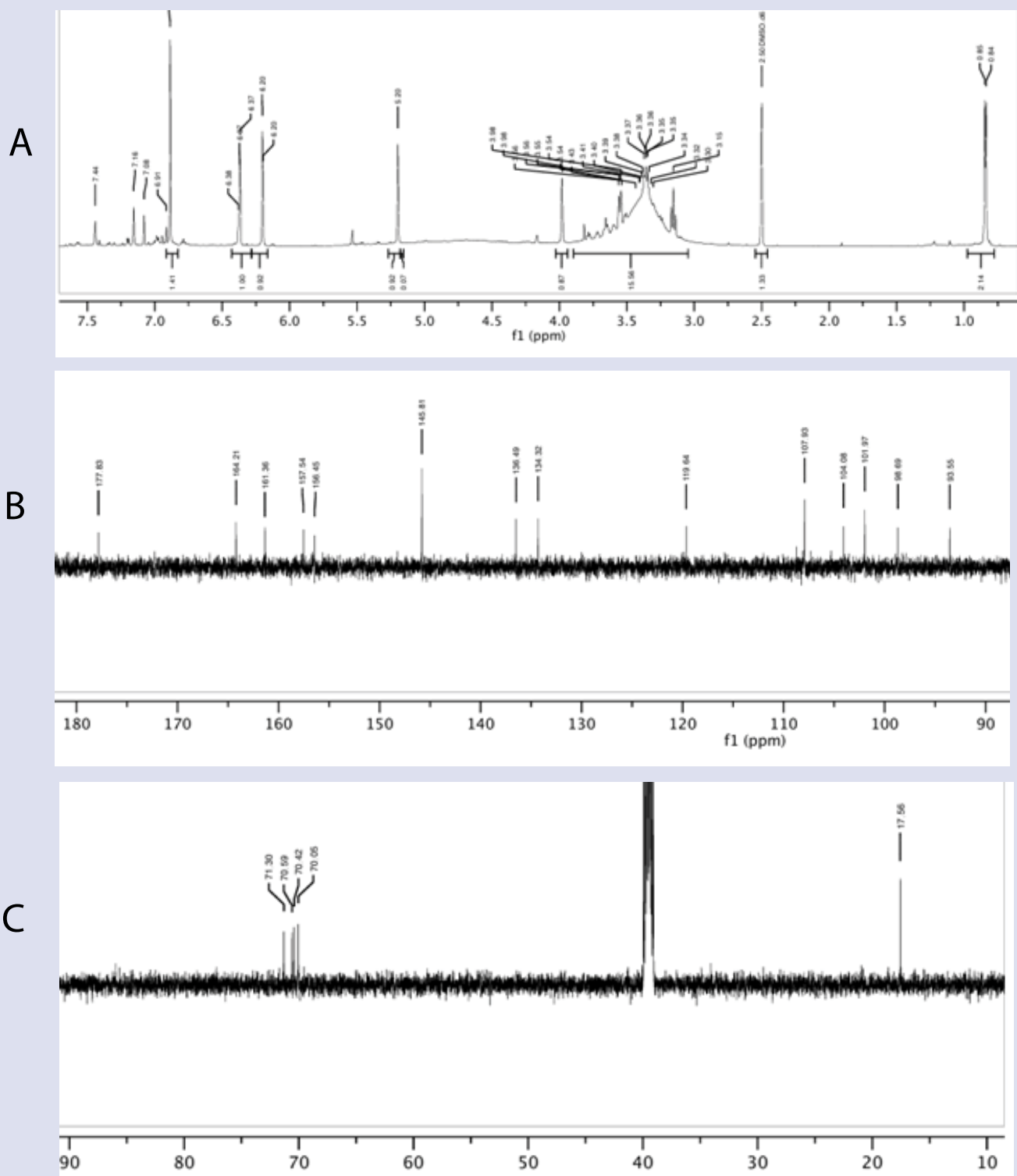


Figure 1. ¹H NMR (A) and ¹³C NMR (B and C) spectra of Myricitrin.

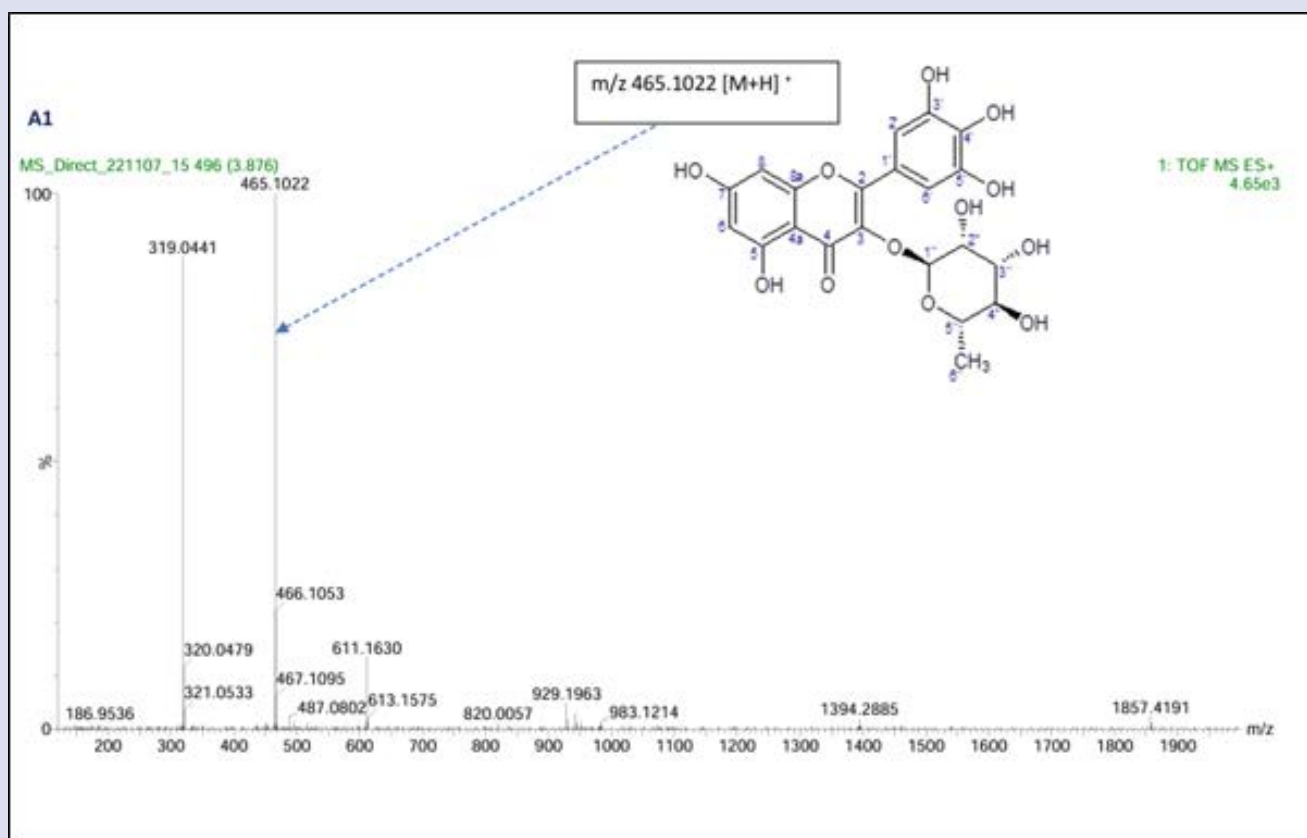


Figure 2. Mass spectrum of isolated flavonoid glycoside (myricitrin).

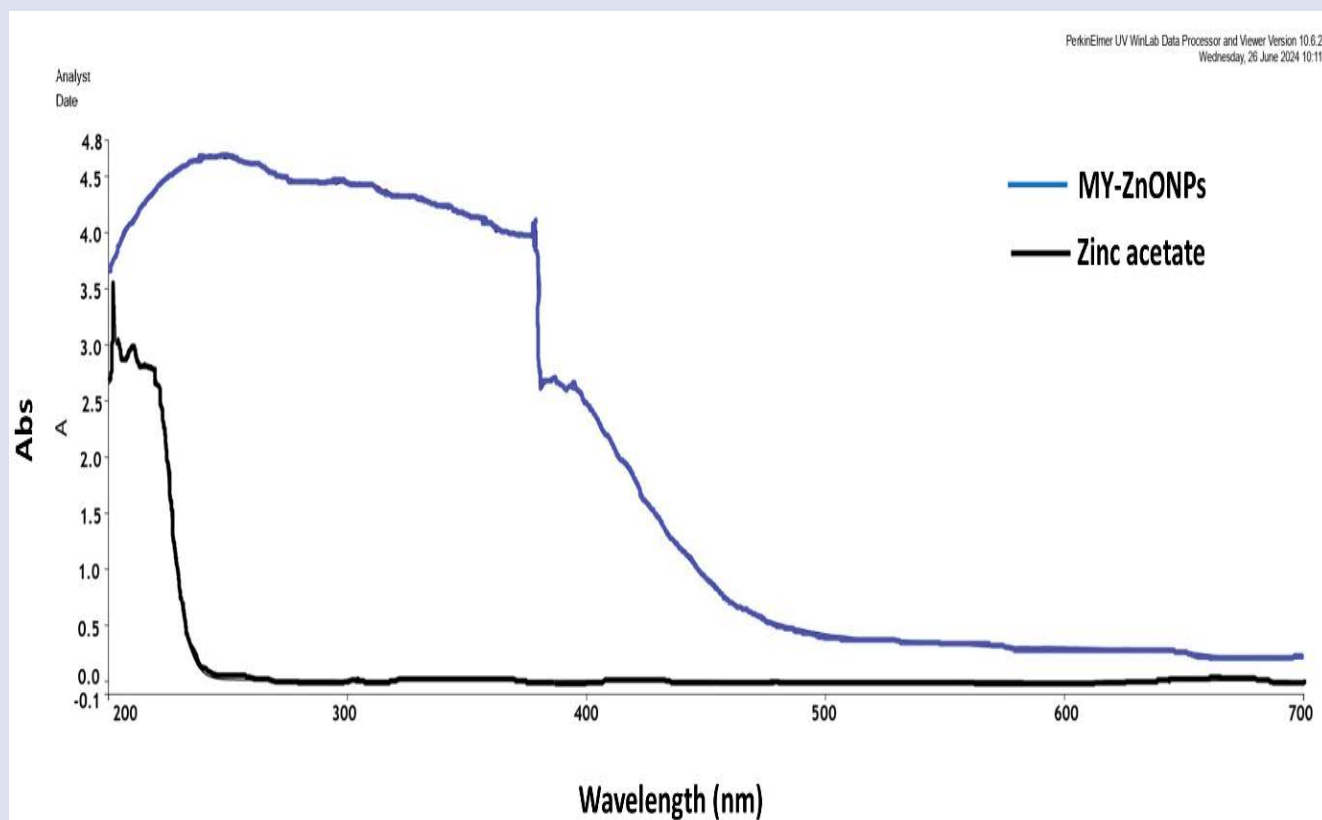


Figure 3. UV-visible spectrum of ZnO nanoparticle synthesized using flavonoid glycoside (MY).

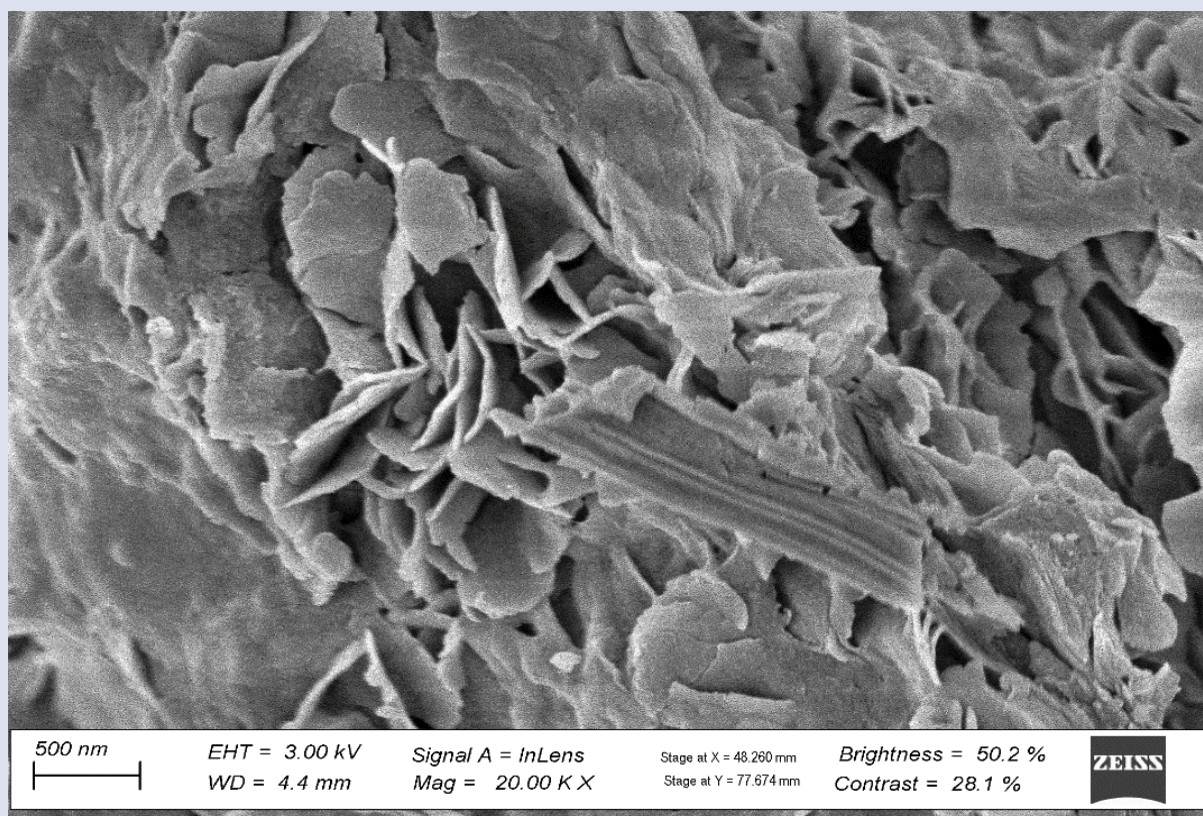


Figure 4. FESEM micrograph analysis of biosynthesized ZnO nanoparticles.

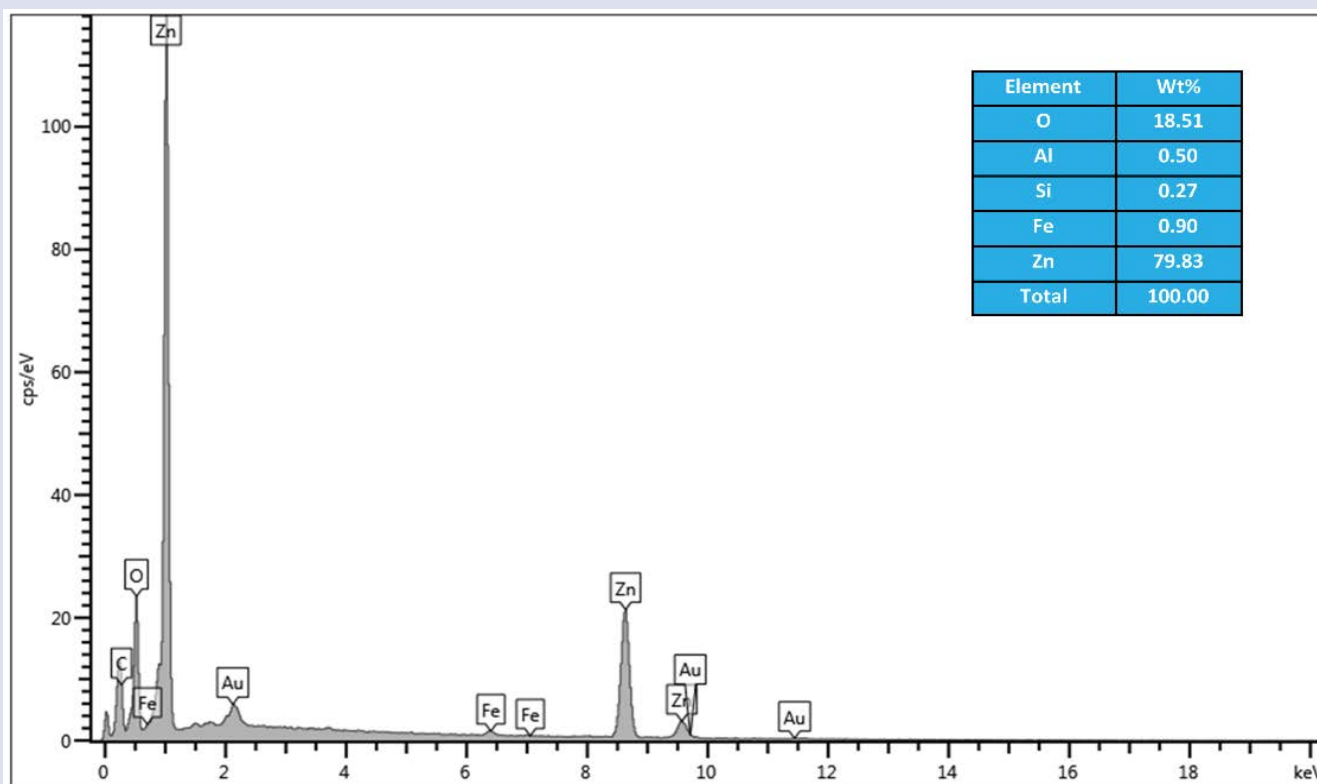


Figure 5. EDX spectrum and elemental profile of biosynthesized nanoparticles.

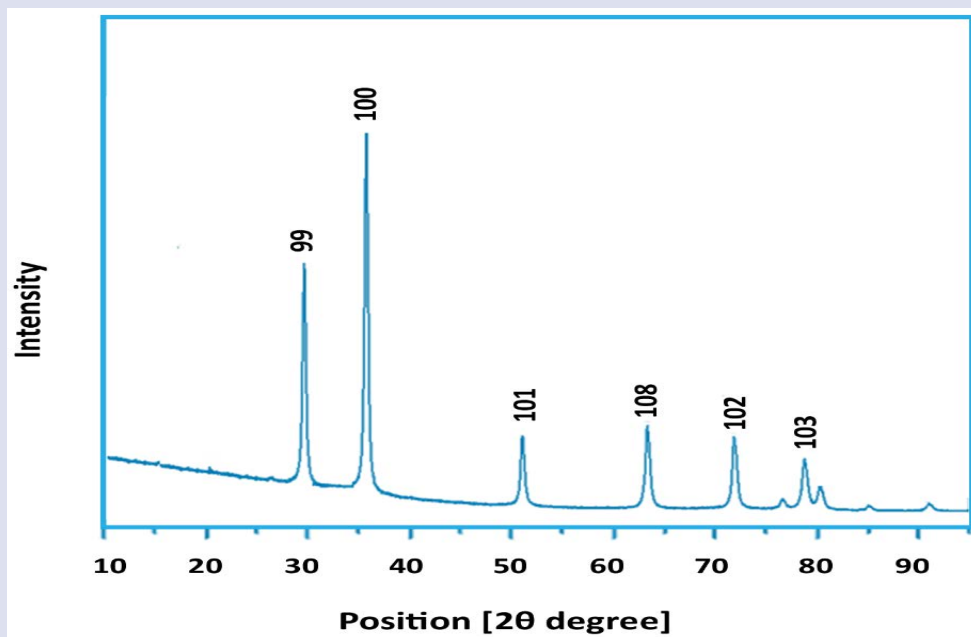


Figure 6. XRD pattern of biosynthesized ZnO nanoparticles.

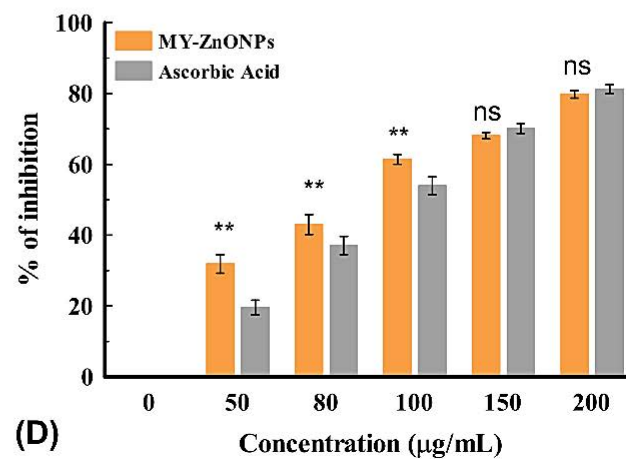
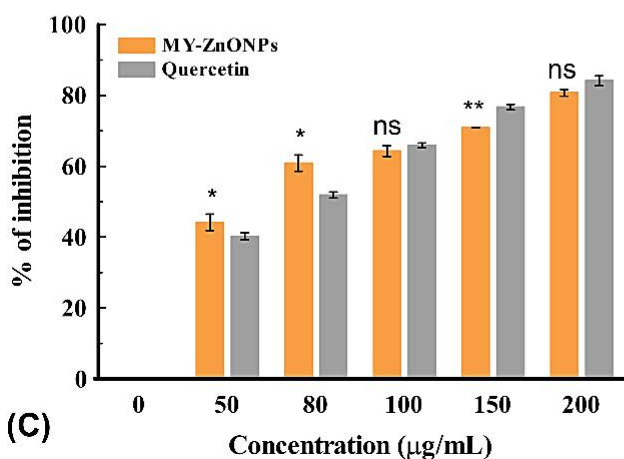
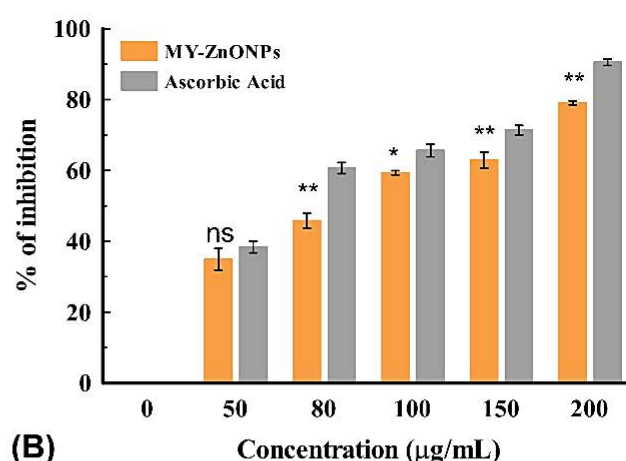
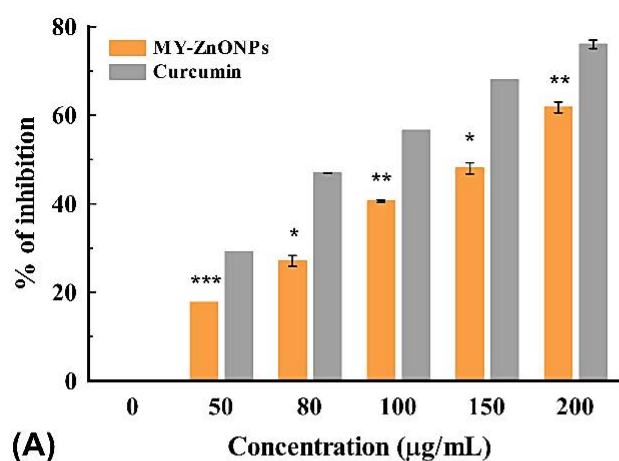


Figure 7. Antioxidant activity of synthesized zinc oxide nanoparticle (A) Nitric oxide. (B) Hydrogen peroxide. (C) Superoxide radical. (D) Hydroxyl radical scavenging activity. [Data expressed as mean \pm S.D. * $p < 0.05$; ** $p < 0.01$; *** $p < 0.001$; NS-Nonsignificant when compared with standard].

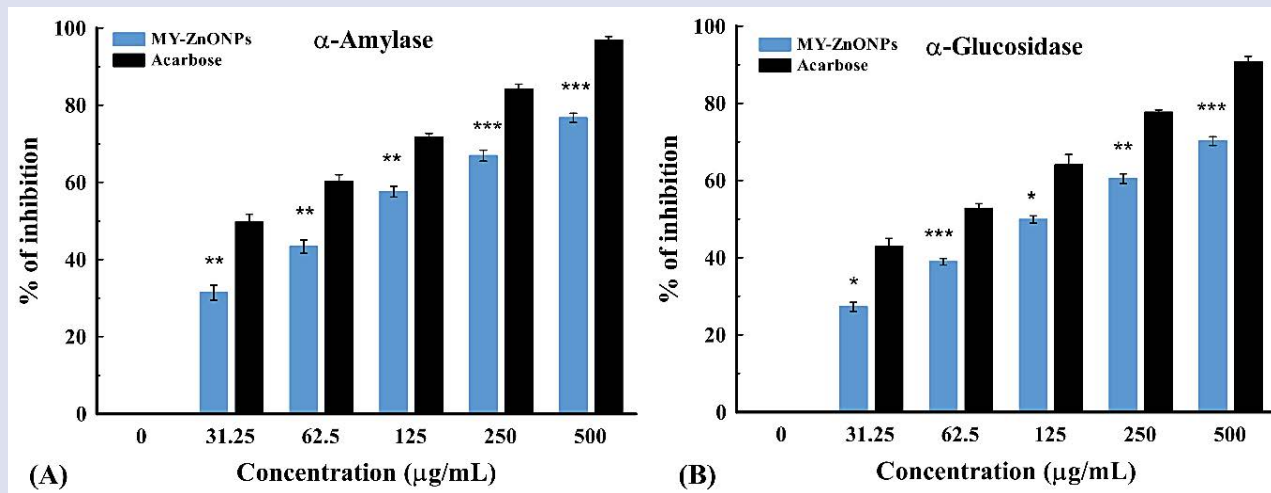


Figure 8. α -Amylase and α -glucosidase inhibition by MY-ZnONPs. [Data expressed as mean \pm S.D. * p <0.05; ** p <0.01; *** p <0.001 when compared with standard].

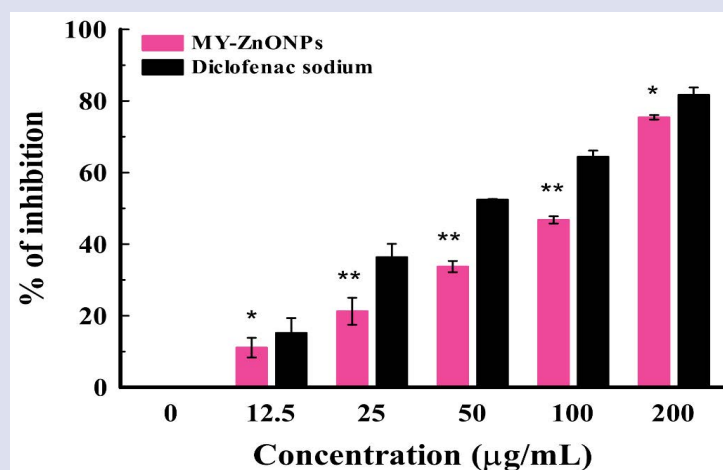


Figure 9. *In vitro* anti-inflammatory activity of the biosynthesized MY-ZnONPs. [Results are given as mean \pm S.D. * p <0.05; ** p <0.01 when compared with standard].

come with adverse side effects^{43,45}. Targeting and slowing the activity of the hydrolyzing enzymes (α -glucosidase and α -amylase) is a crucial strategy for managing diabetes mellitus. Enzymes like α -glucosidase and α -amylase significantly influence the metabolism and absorption of carbohydrates. Therefore, post-prandial hyperglycaemia may be lessened if the activities of these enzymes are inhibited.⁴² The α -glucosidase and α -amylase enzyme activity can be appropriately inhibited by a number of hyperglycaemic medications, such as acarbose, miglitol, and voglibose; however, these medications are known to have side effects.⁴² Due to the drawbacks of these medications, there is currently a great deal of interest in zinc oxide nanoparticle sources of inhibitors with little adverse effects.⁴² In this study, α -glucosidase and α -amylase inhibitory assay was evaluated using the synthesized MY-ZnONPs. A standard drug-acarbose was used as a positive control. It is interesting to note that the MY-ZnONPs inhibited α -amylase and α -glucosidase significantly (p <0.05) in a dose-dependent manner (Figure 8A and B). The NPs exhibited an IC_{50} of $89.24 \pm 0.63 \mu\text{g/mL}$ against α -amylase, which is a significantly lower activity compared to acarbose, the standard anti-diabetic drug ($\text{IC}_{50} = 42.81 \pm 0.51 \mu\text{g/mL}$). Additionally, it inhibited α -glucosidase enzyme at an IC_{50} of $105.95 \pm 0.05 \mu\text{g/mL}$, which

is also lower in activity than acarbose at an IC_{50} of $37.55 \pm 0.05 \mu\text{g/mL}$. The inhibitory activity of ZnONPs against α -glucosidase and α -amylase could be due to compounds capping the nanoparticles⁴⁴. So, the present findings reveal that the MY-ZnONPs have a higher anti-hyperglycaemic effect and could be used in mitigating blood glucose levels.

Anti-inflammatory activity

The denaturation method of the protein egg albumin was applied in this work. The process by which proteins lose their biological structure and function due to inflammation caused by heat, stress, or certain substances is known as protein denaturation. Accordingly, protein denaturation is thought to be a sign of inflammation⁴⁶. The present study assessed how the biosynthesized MY-ZnONPs inhibited the denaturation of albumin and proteins. Even at modest doses, these MY-ZnONPs significantly inhibited albumin denaturation compared to the usual medication, diclofenac sodium salt (Figure 9). Kyene *et al.*⁴⁷ reported that ZnONPs generated by *Cassia sieberiana* inhibited albumin denaturation with an IC_{50} value of 0.676 mg/mL . According to previously reported investigations, synthetic ZnONPs can regulate auto-antigens production and denaturizes proteins during inflammation.

CONCLUSION

This study has delivered robust phytochemical techniques for isolating and characterizing myricitrin as a natural flavonoid glycoside from the medicinally important *E. uniflora* leaf. It also presented a green synthesis method for developing eco-friendly myricitrin-based ZnONPs. Finally, it has been revealed through this study that MY-ZnONPs, a flavonoid glycoside-based metallic nanoparticle, possesses notable antioxidant, anti-hyperglycaemic, and anti-inflammatory activities. Further *in vivo* studies to establish the safety and efficacy of the biogenic nanoparticles as an anti-hyperglycaemic and/or anti-inflammatory agent may be worthwhile.

ACKNOWLEDGMENTS

The authors thank the Research Directorates of Walter Sisulu University (African Medicinal Flora and Fauna Niche Area and PDRFs) and NRF Rated Researcher Incentive for their financial support.

REFERENCES

1. Kavitha KS, Baker S, Rakshith D, Kavitha HU, Yashwantha Rao HC, Harini BP, Satish S. Plants as green source towards synthesis of nanoparticles. *Int Res J Biol Sci.* 2013; 2: 66–76.
2. Malik P, Shankar R, Malik V, Sharma N, Mukherjee TK. Green chemistry based benign routes for nanoparticle synthesis. *J Nanopart.* 2014; 2014: 302429.
3. Kalpana V N, Rajeswari VD. A review on green synthesis, biomedical applications, and toxicity studies of ZnO NPs. *Bioinorg Chem Appl.* 2018; 2018: 3569758.
4. Makarov VV, Love AJ, Sinitsyna OV, Makarova SS, Yaminsky IV, Taliany ME, Kalinina NO. "Green" nanotechnologies: synthesis of metal nanoparticles using plants. *Acta Naturae.* 2014; 6: 35-44.
5. Arya V. Living systems: Eco-friendly nanofactories. *Dig J Nanomater Bios.* 2010; 5: 9–21.
6. Biswas B, Rogers K, Mclaughlin F, Daniels D, Yadav A. Antimicrobial activities of leaf extracts of Guava (*Psidium guajava* L.) on two Gram-negative and Gram-positive bacteria. *Int J Microbiol.* 2013; 2013: 746165.
7. Mittal AK, Chisti Y, Banerjee UC. Synthesis of metallic nanoparticles using plant extracts. *Biotechnol Adv.* 2013; 31: 346-356.
8. Rajan R, Chandran K, Harper SL, Yun SI, Kalaichelvan PT. Plant extract synthesized silver nanoparticles: An ongoing source of novel biocompatible materials. *Ind Crop Prod.* 2015; 70: 356–373.
9. Ahmed S, Ahmad M, Swami BL, Ikram S. A review on plants extract mediated synthesis of silver nanoparticles for antimicrobial applications: A green expertise. *J Adv Res.* 2016; 7: 17–28.
10. Fan ZY, Lu JG. Zinc oxide nanostructures: Synthesis and properties. *J Nanosci Nanotechnol.* 2005; 5: 1561–1573.
11. Dey S, Lochan Mohanty D, Divya N, Bakshi V, Mohanty A, Rath D, Das S, Mondal A, Roy S, Sabui R. A critical review on zinc oxide nanoparticles: Synthesis, properties and biomedical applications. *Intelligent Pharm.* 2025; 3: 53–70.
12. Saeed M, Marwani HM, Shahzad U, Asiri AM, Rahman MM. Recent advances, challenges, and future perspectives of ZnO nanostructure materials towards energy applications. *The Chemical Record.* 2024; 24: e202300106.
13. Divya MJ, Sowmia C, Joon K, Dhanya KP. Synthesis of zinc oxide nanoparticle from *Hibiscus rosa-sinensis* leaf extract and investigation of its antimicrobial activity. *Res J Pharm Biol Chem Sci.* 2013; 4: 1137–1142.
14. Ramesh P, Rajendran A, Sundaram M. Green synthesis of zinc oxide nanoparticles using flower extract *Cassia Auriculata*. *J Nanosci Nanotechnol.* 2014; 2: 41–45.
15. Wang H, Du YJ, Song HC. α -Glucosidase and α -amylase inhibitory activities of guava leaves. *Food Chem.* 2010; 123: 6–13.
16. Tang X, Zhang C, Chen M, Xue Y, Liu T, Xue W. Synthesis and antiviral activity of novel myricitrin derivatives containing ferulic acid amide scaffolds. *New J Chem.* 2020; 44: 2374–2379.
17. Zhang C, Zhang G, Liao Y, Gong D. Myricetin inhibits the generation of superoxide anion by reduced form of xanthine oxidase. *Food Chem.* 2017; 221: 1569–1577.
18. Ha TK, Jung I, Kim ME, Bae SK, Lee JS. Anti-cancer activity of myricetin against human papillary thyroid cancer cells involves mitochondrial dysfunction-mediated apoptosis. *Biomed Pharmacother.* 2017; 91: 378–384.
19. Trung HT, Huynh H TT, Thuy LNT, Minh HNV, Nguyen MN, Thi MNL. Growth-inhibiting bactericidal antibiofilm and urease inhibitory activities of *Hibiscus rosa sinensis* I Flower constituents toward antibiotic sensitive- and resistant-strains of *Helicobacter pylori*. *ACS Omega.* 2020; 5: 20080–20089.
20. Zhang X, Zhang K, Wang Y, Ma R. Effects of myricitrin and relevant molecular mechanisms. *Curr Stem Cell Res & Therapy.* 2020; 15: 11-17.
21. Fidelis EM, Savall ASP, de Oliveira Pereira F, Quines CB, Ávila DS, Pinton S. Pitanga (*Eugenia uniflora* L.) as a source of bioactive compounds for health benefits: A review. *Arabian J Chem.* 2022; 15: 103691.
22. Oriola AO, Miya GM, Singh M, Oyedeji AO. Flavonol glycosides from *Eugenia uniflora* leaves and their *in vitro* cytotoxicity, antioxidant and anti-inflammatory activities. *Scientia Pharma.* 2023; 91: 42.
23. Naseer M, Aslam U, Khalid B, Chen B. Green route to synthesize Zinc Oxide Nanoparticles using leaf extracts of *Cassia fistula* and *Melia azadarach* and their antibacterial potential. *Sci Rep.* 2020; 10: 1-10.
24. Garratt DC. *The Quantitative Analysis of Drugs.* Chapman and Hall Ltd Springer Japan 1964.
25. Long LH, Evans PJ, Halliwell B. Hydrogen peroxide in human urine: implications for antioxidant defense and redox regulation. *Biochem Biophys Res Commun.* 1999; 262: 605–609.
26. Kunchandy E, Rao MNA. Oxygen radical scavenging activity of curcumin. *Int J Pharm.* 1990; 58: 237-240.
27. Fontana M, Mosca L, Rosei MA. Interaction of enkephalins with oxyradicals. *Biochem Pharmacol.* 2001; 61: 253–257.
28. Wickramaratne MN, Punchihewa JC, Wickramaratne DBM. *In vitro* alpha amylase inhibitory activity of the leaf extracts of *Adenanthera pavonina*. *Appl Microbiol Biotechnol.* 2016; 16: 1–6.
29. Rengasamy KR, Aderogba MA, Amoo SO, Stirk WA, VanStaden J. Potential antiradical and alpha- glucosidase inhibitors from *Ecklonia maxima* (Osbeck) Papenfuss. *Food Chem.* 2013; 4: 1412–1415.
30. Kassem MES, Ibrahim F, Hussein SR, El-Sharawy R, El-Ansari MA, Hassanane MM, Booles HF. Myricitrin and bioactive extract of *Albizia amara* Leaves: DNA protection and modulation of fertility and antioxidant-related genes expression. *Pharm Biol.* 2016; 54: 2404–2409.
31. Chinnasamy E, Indumathi N, Deepa K, Madhavan J, Senthil S. Growth and characterization of zinc acetate dihydrate formic acid single crystals. *Res J Pharm Biol Chem.* 2017; 8: 2030–2035.
32. Polash SH, Pyreddy S, Abraham AN, Mahasivam S, Bansal V, Varadi L, Bryant G, Shukla R. Impact of nucleic acid encapsulated MOF crystal phase on protein corona formation. *Mater Adv.* 2023; 4: 4761–4774
33. Naiel B, Fawzy M, Halmy MWA, Mahmoud AEID Green synthesis of zinc oxide nanoparticles using sea lavender (*Limonium pruinosum* L. Chaz.) extract: Characterization, evaluation of anti-skin cancer, antimicrobial and antioxidant potentials. *Sci Rep.* 2022; 12: 20370.

34. Fakhari S, Jamzada M, Fard HK. Green synthesis of zinc oxidenanoparticles: A comparison. *Green Chem Lett Rev.* 2019;12(1):19–24.
35. El-Belely EF, Farag MM, Said HA, Amin AS, Azab E, Gobouri AA, Fouda A. Green synthesis of zinc oxide nanoparticles (ZnO-NPs) using *Arthrospira platensis* (Class: Cyanophyceae) and evaluation of their biomedical activities. *Nanomaterials.* 2021; 11: 95
36. Elumalai K, Velmurugan S. Green synthesis, characterization and antimicrobial activities of zinc oxide nanoparticles from the leaf extract of *Azadirachta indica* (L.). *Appl Surf Sci.* 2015; 345: 329-336.
37. Albarakaty FM, Alzaban MI, Alharbi NK, Bagrwan FS, Abd El-Aziz ARM, Mahmoud MA. Zinc oxide nano-particles, biosynthesis, characterization and their potent photocatalytic degradation, and antioxidant activities. *J King Saud Univ Sci.* 2023; 35: 102434.
38. Jamzad SFM, Fard HK. Green synthesis of zinc oxide nanoparticles: a comparison. *Green Chem Lett Rev.* 2019; 12: 19–24
39. Khan AU, Malik N, Singh B, Ansari NH, Rehman M, Yadav A. Biosynthesis, and characterization of zinc oxide nanoparticles (ZnONPs) obtained from the extract of waste of strawberry. *J Umm Al-Qura Univ Appl Sci.* 2023; 9: 268–275.
40. Mates JM, Sanchez-Jimenez FM. Role of reactive oxygen species in apoptosis: implications for cancer therapy. *Int J Biochem Cell Biol.* 2000; 32: 157–170.
41. Bhakya S, Muthukrishnan S, Sukumaran M, Muthukumar M. Biogenic synthesis of silver nanoparticles and their antioxidant and antibacterial activity. *Appl Nanosci.* 2016; 6: 755–766.
42. Rehana D, Mahendiran D, Kumar RS, Rahiman AK. In vitro antioxidant and antidiabetic activities of zinc oxide nanoparticles synthesized using different plant extracts. *Bioprocess Biosyst Eng.* 2017; 40(6): 943–957.
43. Gadoa ZA, Moustafa AH, El Rayes SM, Arisha AA, Mansour MF. Zinc oxide nanoparticles and synthesized pyrazolopyrimidine alleviate diabetic effects in rats induced by type II diabetes. *ACS Omega.* 2022; 7: 36865–36872.
44. Kifle ZD, Enyew EF. Evaluation of *in vivo* antidiabetic, *in vitro* α -amylase inhibitory, and *in vitro* antioxidant activity of leaves crude extract and solvent fractions of *Bersama abyssinica* fresen (melianthaceae). *J Evid-Based Integr Med.* 2020; 25: 2515690X20935827
45. Haase H, Overbeck S, Rink L. Zinc supplementation for the treatment or prevention of disease: current status and future perspectives. *Exp Gerontol.* 2008; 43: 394–408.
46. Altir NKM, Ali AMA, Gaafar ARZ, Qahtan AA, Abdel-Salam EM, Alshameri A, Hodhod MS, Almunqedhi B. Phytochemical profile, *in vitro* antioxidant, and anti-protein denaturation activities of *Curcuma longa* L. rhizome and leaves. *Open Chem.* 2021; 19: 945-952.
47. Kyene MO, Droepenu EK, Ayertey F, Yeboah GN, Archer MA, Kumadoh D, Mintah SO, Gordon PK, Appiah AA. Synthesis and characterization of ZnO nanomaterial from *Cassia sieberiana* and determination of its anti-inflammatory, antioxidant and antimicrobial activities. *Sci African.* 2023; 19: e01452.

Cite this article: Pallab K, Ayodeji O O, Adebola O O. Natural Flavonoid Glycoside-Based Zinc Oxide Nanoparticles: Compound Isolation, Nanoparticle Green Synthesis, Characterization, and *in vitro* Antioxidant, Anti-hyperglycaemic and Anti-inflammatory Effects. *Pharmacogn J.* 2025;17(5): 531-541.